Polímeros
ISSN 1678-5169 (Online)

https://doi.org/10.1590/0104-1428.20220123

ORIGINAL ARTICLE

Ternary segmented polyurethanes: morphology and kinetics of the crystallization

André Sanches Bevilacqua[1], Rafael Bergamo Trinca[1] and Maria Isabel Felisberti[1]*

[1]Instituto de Química, Universidade Estadual de Campinas – UNICAMP, Campinas, SP, Brasil
misabel@unicamp.br

Abstract

Segmented polyurethanes based on poly(l-lactide)diol – PLLA, poly(ethylene-glycol) – PEG, poly(trimethylene-carbonate)diol – PTMC and hexamethylene diisocyanate were synthesized by a two-step polyaddition. Polyurethanes with variable compositions and molar mass were semi-crystalline and presented PLLA or PLLA + PEG crystalline phases and a heterogeneous amorphous phase. Sequential crystallization of PLLA and PEG resulted in a confined PEG crystallization into the PLLA crystalline phase. The random distribution of the segments in the polymer chains and the partial miscibility of the segments in the amorphous phase strongly influenced the morphology of the crystalline phase, and the kinetics of the crystallization. Morphology changed from not well-defined spherulites with Maltese cross to ring banded spherulites and axialites as the PLLA mass fraction decreased. PLLA nucleation and crystal growth rates varied with crystallization temperature similarly to homopolymers, presenting a bell-shaped curve, and the temperature for the maximum growth rate dependent on the polyurethanes composition.

Keywords: *crystallization, kinetics, morphology, segmented polyurethanes.*

How to cite: Bevilacqua, A. S., Trinca, R. B., & Felisberti, M. I. (2023). Ternary segmented polyurethanes: morphology and kinetics of the crystallization. *Polímeros: Ciência e Tecnologia*, *33*(1), e20230008. https://doi.org/10.1590/0104-1428.20220123

1. Introduction

Crystallization is an important issue in polymer science because this process is amenable to be tailored to improve properties[1]. The crystallization of polymers is complex, and the complexity is even greater for blends and copolymers due to factors such as the interactions among different segments, volume fraction and the molar mass of the crystallizable polymers, and phase separation[2-7]. Different crystalline structures may be observed in blends and copolymers of varied compositions and crystallization conditions[3-5]. For copolymers, phase separation results in microphases in which crystallization occurs[2,5,8]. One of the most studied block copolymer is poly(ethylene glycol)-*b*-poly(L-lactide), PEG-*b*-PLLA, because blocks crystallize[5,9,10]. Moreover, PEG crystallizes in confined environments within the PLLA crystalline structure[8-15].

Another class of copolymers is that of segmented polyurethanes (SPU). In general, these polyurethanes are prepared using different macrodiols that constitute blocks in the polyurethane chains. The main difference between SPU and traditional block copolymers is that, in SPU, the blocks are random distributed along the polymer chains. Despite their random architecture, SPU present microphase separation and the resulting phases are capable of crystallization[16-20]. The combination of a great variety of precursors imparts to SPU properties that make them useful in a variety of applications[21]. The combination of two or three macrodiols results in binary and ternary SPU, respectively[22,23]. The properties of SPU are defined by the characteristics of the macrodiols (e.g., hydrophilicity, crystallinity), of the diisocyanates (aromatic, aliphatic and cycloaliphatic), and chain extenders[21,24-28]. In general, semi-crystalline soft segments may crystallize if they are connected to symmetric diisocyanate and in conditions of low steric hindrance[29,30]. High diisocyanate contents (> 50 wt%) may inhibit soft segment crystallization[19].

Ternary SPU based on PEG, PLLA and poly(trimethylene carbonate) (PTMC) macrodiols and hexamethylene diisocyanate (HDI) or toluene diisocyanate (TDI) have been studied by our research group[22,23]. The combination of the properties of PEG (a semi-crystalline and hydrophilic polyether), PLLA (a semi-crystalline and hydrophobic polyester), and PTMC (an amorphous and hydrophobic polycarbonate) segments in variable mass fractions allowed the syntheses of amphiphilic SPU with a wide range of properties that depend heavily on composition.

The miscibility of PLLA and PEG is controversial. Many reports on PLLA/PEG blends[31] and copolymers[9] have suggested that they are immiscible. However, PEG and PLLA may be miscible in the molten state for block copolymers[9,13]. PLLA and PTMC are reported as immiscible[32] or partially miscible[33], while PEG and PTMC are miscible[34]. In PEG/PLLA blends and PEG-*b*-PLLA diblock copolymers, PEG chains or blocks, respectively, influence the crystallization of PLLA from the molten state, reduce the PLLA number

of nuclei, and increase the PLLA spherulite growth rate[15]. Because the melting and crystallization temperatures of PEG are lower than the crystallization temperature for PLLA, in the cooling from the molten state, PLLA crystallizes first and PEG crystallizes in confined environments of the PLLA crystalline phase[5,31]. In PLLA/PTMC blends, PTMC decreases the PLLA spherulite growth rate and increases the PLLA number of nuclei[32].

The phase behavior of the SPU based on PLLA, PEG and PTMC is quite complex. Based on thermal, dynamic mechanical properties and morphology, Trinca and Felisberti concluded that PTMC may promote partial miscibility of the PEG and PLLA segments[22,23].

In this work, we studied the crystallization of ternary SPU based on PEG, PLLA, PTMC and hexamethylene diisocyanate. Ternary SPU with different PLLA, PEG and PTMC mass fractions were synthesized via the two-step route and isothermal crystallization was conducted by cooling from the molten state to the crystallization temperature of the PLLA, followed by the crystallization of PEG segments induced by further cooling. The morphology of the SPU was studied by polarized optical microscopy (POM) and atomic force microscopy (AFM). The kinetics of crystallization of the PLLA segments in the SPU was evaluated by POM and the effect of the polyurethane composition on the nucleation and growth rates was discussed. To the best of our knowledge, there are no reports on the crystallization behavior of ternary SPU based on two semi-crystalline blocks such as PEG and PLLA.

2. Experimental

2.1 Homopolymers and polyurethanes synthesis and characterization

Tin (II) 2-ethylhexanoate (92.5%–100% purity), dibutyltin dilaurate (DBTDL, 95%), hexamethylene diisocyanate (HDI, 98%), 1,4-butanediol (BD), 3,6-dimethyl-1,4-dioxan-2,5-dione (L-lactide, LLA, 98%) and PEG (2kDa) were purchased from Sigma Aldrich. 1,3-dioxan-2-one (trimethylene carbonate, TMC) was purchased from Boehringer Ingelheim. PLLA and PTMC macrodiols were synthesized by ring-opening polymerization (ROP) using the procedure previously reported[35]. Based on our previous works[22,23], SPU were synthesized using PEG (M_n = 2.0 kDa, Mw/Mn= 1.1; hydroxyl index I_{OH} = 0.95 mmol g^{-1}), PLLA (M_n = 2.5 kDa, Mw/Mn= 1.2; hydroxyl index I_{OH} = 0.80 mmol g^{-1} or M_n = 4.1 kDa, Mw/Mn= 1.2; I_{OH} = 0.49 mmol g^{-1})) and PTMC (M_n = 2.4 kDa, Mw/Mn= 1.8; I_{OH} = 0.83 mmol g^{-1}) macrodiols, HDI as diisocyanate, and BD as chain extender by a two-step route. The macrodiols and SPU were characterized by gel permeation chromatography (GPC), hydrogen nuclear magnetic resonance (^{1}H NMR) and differential scanning calorimetry (DSC); the results are summarized in Table 1. DSC analyses were performed on an MDSC2910 (TA Instruments) using the following sequence at a heating and cooling rate of 20 °C min^{-1}: i) heating from 25 °C to 200 °C; ii) 2 min isotherm; iii) cooling from 200 °C to -100 °C; iv) 2 min isotherm; v) second heating from -100 °C to 200 °C.

2.2 Kinetics of crystallization and morphology

Kinetics of the crystallization and the morphology of the crystalline phase were studied by POM using a Nikon Eclipse 80i optical microscope coupled to a Linkam CSS-450 hot stage and a Nikon DS camera D2 U2. Thin PLLA-diol (M_n = 4.2kDa) and SPU films of thicknesses varying from 10 µm to 30 µm and area of 1.5 x 1.5 cm^2 were prepared by solvent casting from a previously filtered 5 wt % solution in $CHCl_3$, using a PTFE filter with a pore diameter of 0.24 µm. Around 200 µL of the solution were deposited on a microscope followed by solvent evaporation. The films were subjected to the crystallization protocol using a Linkam hot stage: i) heating from room temperature to 180 °C at 10 °C min^{-1}; ii) isotherm for 2 min; iii) cooling at 20 °C min^{-1} to the crystallization temperature for PLLA (T_{cPLLA}); iv) isotherm at T_{cPLLA} for 1 h to crystallize PLLA segments; v) cooling to 40 °C (T_{cPEG}) at 20 °C min^{-1}; vi) 30 min isotherm at 40 °C to crystallize PEG segments. Crystallization temperatures for PLLA segments in the SPU and PLLA-diol were 75, 80, 85, 90, 95, 100, 105, 110, and 115 °C. For PLLA-diol, steps i, ii, iii, and iv were performed and the crystallization was conducted for around 10 min. For each crystallization experiment, images were captured at each 10 s using a Nikon microscope software NIS Elements AR.

For AFM analysis, films prepared as described for POM analysis, and with 10 µm thickness were isothermally crystallized using a Linkam CSS-450 hot stage. The crystallization protocol was heating at the rate of 10 °C min^{-1} from room temperature to 180 °C, isotherm for 2 min, and cooling at the rate of 20 °C min^{-1} to the crystallization temperature of the PLLA, T_{cPLLA} = 100 °C through 1 h. It was followed by further cooling to crystallize PEG at T_{cPEG} = 40 °C for

Table 1. Mass fraction of the macrodiol "i" (x_i) in the SPU, molar mass and dispersity, and thermal properties of the SPU.

SPU	x_{PEG} [a]	x_{PLLA} [a]	x_{PTMC} [a]	M_n [b] (kDa)	M_w/M_n [b]	T_{cPEG} [c] (°C)	T_{cPLLA} [c] (°C)	T_g [d] (°C)	T_{cPEG} [e] (°C)	T_{mPEG} [e] (°C)	T_g [f] (°C)	T_c [f] (°C)	T_m [f] (°C)
SPU111	0.32	0.33	0.35	11.0	1.8	17	92	-24	22	-	-	85	72; 117
SPU121	0.25	0.45	0.30	11.0	1.8	-	96	-13	38	-	-	96	78; 125
SPU112	0.26	0.25	0.49	12.0	2	35	86	-25	28	-	-	91	73; 122
SPU211	0.44	0.23	0.33	14.0	1.8	16	93	-36	10	34	-	91	123
SPU163	0.11	0.59	0.30	11.0	3.2	-	82	2	-	-	74	-	123
SPU299	0.11	0.42	0.47	10.0	3.6	-	85	-6	-	-	74	-	123

[a]Mass fraction of the macrodiols in relation to the total mass of the macrodiols in the SPU (determined by 1H NMR). [b]Determined by GPC. [c]Crystallization temperature determined in cooling scans. [d]Glass transition temperatures of the SPU determined in the second heating scans. [e]Crystallization and melting temperatures of the PEG phase and [f] glass transition, crystallization and melting temperatures of the PLLA phase determined in the second heating scans.

30 min. The samples were examined on an Atomic Force Microscope Nanosurf C3000 Nanoscope, operating in tapping mode with a Si probe Nanoworld FMR (resonance frequency 75 kHz and constant force of 2.8 Nm^{-1}) at the Laboratory of Surface Science (LSC) – CNPEM.

3. Results and Discussion

The nomenclature, composition expressed in mass fraction, number average molar mass M_n, and dispersity D are presented in Table 1. The nomenclature used for the polyurethanes, SPUxyz, describes the mass proportion of each segment: x = PEG; y = PLLA and z = PTMC. In general, the SPU presented M_n in the range of 11 kDa – 14 kDa.

The crystallization of the macrodiol segments in the SPU depends on their length and isocyanate content[16,19]. According to Li et al.[16], SPU based on polycaprolactone diol, 4,4'-diphenylmethane diisocyanate (MDI) and 1,4-butanediol did not crystallize if the molar mass of the macrodiol was lower than 2 kDa. Concerning diisocyanate content, high diisocyanate mass fraction (≥ 50%) in the SPU led to the crystallization of the diisocyanate-HDI segments and confined the crystallization of PEG into HDI crystalline structure[19].

The molar masses of the PEG (M_n = 3.0 kDa) and PLLA (M_n = 2.5 kDa, and 4.1 kDa) crystallizable segments, the low diisocyanate content in the SPU in the range of 7-21%, the symmetry and the low hysteric hindrance imparted by aliphatic nature of the HDI, favor the crystallization of these segments in the SPU[29,30]. DSC analyses revealed thermal events associated with PEG and PLLA crystalline and amorphous phases in the SPU, as shown in Figure 1. DSC data such as glass transition temperature (T_g), crystallization and melting temperatures (T_c and T_m, respectively) are summarized in Table 1.

During the DSC cooling from the molten state, PLLA segments crystallized in the range of 82-96 °C for all SPU. However, PEG crystallization below 50 °C was verified only for SPU111, SPU112, and SPU211 (Figure 1a) in the range of 10-35 ° C. Apparently, a minimum mass fraction of PEG (> 0.11) is necessary for an appreciable crystallization under the cooling conditions. SPU composition influences slightly the crystallization temperatures of the PLLA phase. DSC 2nd heating scan of the SPU163 and SPU299 (Figure 1b) presented a glass transition around 2° C and -6 °C, respectively, attributed to an amorphous phase composed of a mixture of randomly connected macrodiols segments[22]; a second and less intense glass transition at 74 °C, attributed to the amorphous phase of PLLA[36], an exothermic peak around 99 °C due to the cold crystallization of PLLA and two melting peaks partially overlapped and above 100 °C due to the melting of PLLA. No peaks related to PEG crystallization (Figure 1a) and melting (Figure 1b) could be observed probably due to the low PEG mass fraction (0.11), random segment-distribution and low chain mobility[22,35]. The presence of two glass transitions indicates that SPU163 and SPU299 are heterogeneous. DSC 2nd heating scans of the others SPU presented a more complex profile, exhibited glass transition, and multiple cold crystallizations and melting peaks (Figure 1b). Glass transition was observed in a temperature range from -50 °C to 25 °C (Figure 1b), and attributed to an amorphous phase constituted by various randomly connected macrodiols[22]. In general, PEG and PTMC segments contributed to a decrease in the glass transition temperature as observed in SPU rich in PEG (211 and 111) and PTMC (111 and 112), which presented the lowest T_g in the range of -36 °C – -24 °C. The cold crystallization of PEG segments occurred above 0 °C and the area and position of the peak depended on the SPU composition (Figure 1b). PEG melting peak was clearly observed for SPU 211 at 34 °C; for the others SPU, the melting is probable overlapped by the PLLA thermal events. The cold crystallization, recrystallization and melting of the PLLA phase, occurred in the temperature range of 40-130 °C. For PLLA, the temperature corresponding to the minimum of the peak at the highest temperature range occurred in a narrow temperature range of 117-125 °C and was not affected by the SPU composition.

According to DSC data, SPU are heterogeneous polymers that present crystalline phases and at least two amorphous phases, depending on their composition. Dynamic mechanical analyses (Figure S1, Supplementary Material) and AFM phase contrast images for SPU (Figure S2) revealed the multiphasic nature of the SPU and the presence of phases with a gradient of composition. In a previous work, dynamic mechanical and AFM analyses showed that ternary SPU were composed

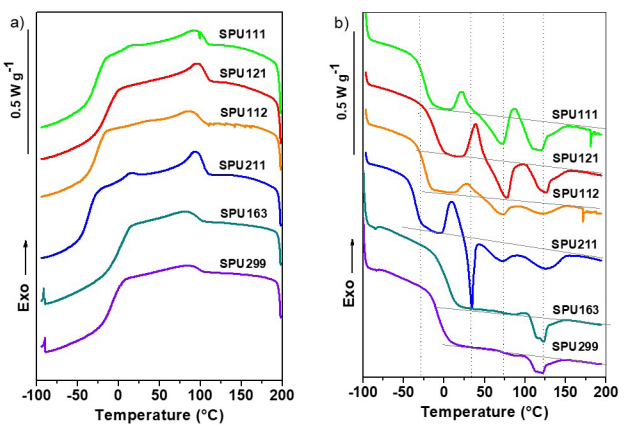

Figure 1. (a) Cooling; (b) 2nd heating DSC scans for SPU.

of PEG-PTMC-rich domains dispersed in an amorphous, continuous, and PLLA-rich phase[22,23]. The increase in the PTMC content resulted in diffuse PEG-PTMC domains suggesting that higher PTMC content promoted partial miscibility of PEG and PLLA[22,23].

Crystallization studies performed by POM allowed the evaluation of the morphology of the crystalline phases in the SPU subjected to isothermal crystallization in the temperature range of 75-115 °C for PLLA, followed by cooling at a rate of 20 °C min^{-1} to 40 °C for PEG crystallization. Figure 2 shows POM images of SPU111 crystallized at different temperatures. The increase in the crystallization temperature for SPU111 resulted in a morphology evolution from spherulites with a Maltese cross at T_c = 75 °C (Figure 2a) into ring banded spherulites at T_c in the range of 80-100 °C (Figures 2b-2f) and finally to axialites at T_c in the range of 105-115 °C (Figures 2g-2i). The evolution of the crystalline phase of the PLLA in the SPU111 is similar to the ones reported for PEG-*b*-PLLA diblock copolymers (M_{nPEG} = 5 kDa[9,13,15] and M_{nPLLA} = 2.5 kDa[13], 3 kDa[15], 5 kDa[9,13-15], 12 kDa[15], and 16 kDa[13]), for which the changes in the morphology were attributed to the evolution of microphase separation between PEG and PLLA at the crystallization temperature. This suggests that the crystallization in SPU is also controlled by phase separation. The occurrence of the ring banded spherulites in the PLLA block of the PEG-*b*-PLLA diblock copolymers with M_{nPEG} = 5 kDa and M_{nPLLA}= 5 kDa and 15kDa crystallized at lower temperatures was due to the twisting of the lamellae caused by the non-crystallizable amorphous phase during crystallization[5]. In SPU, the cause of the lamellar twisting may the presence of a complex molten amorphous phase constituted by PLLA, PEG and PTMC.

The morphology of the PLLA crystalline phase in SPU211 (Figure S3) varied in a similar way to that observed in SPU111 (Figure 2). In SPU121, spherulites with Maltese cross were observed in samples crystallized in the temperature range of 90-100 °C (Figure S4). The increase in the PTMC mass fraction led to the formation of ring banded PLLA spherulites in SPU112 at crystallization temperatures below 100 °C (Figure S5). Moreover, PLLA-diol used to synthesize SPU presented well-defined spherulites with Maltese cross at the crystallization temperature of up to 90 °C, ring banded spherulites up to 110 °C and an axialites-like structure at 115 °C (Figure S6). These results show that the PLLA crystalline phase may present similar morphology if PLLA-diol and SPU are crystallized at different temperatures. Therefore, the profile of the nucleation rate and crystal growth rate as a function of temperature is governed by the composition. POM images of SPU163 and SPU299 are shown in Figures S7 and S8, respectively.

The PLLA phase for the SPU211 crystallized as axialites at 105 °C (Figure 3a). Further cooling to 40 °C led to PEG crystallization in and around the axialites (Figure 3b) and showed that the PLLA crystalline phase acted as a template

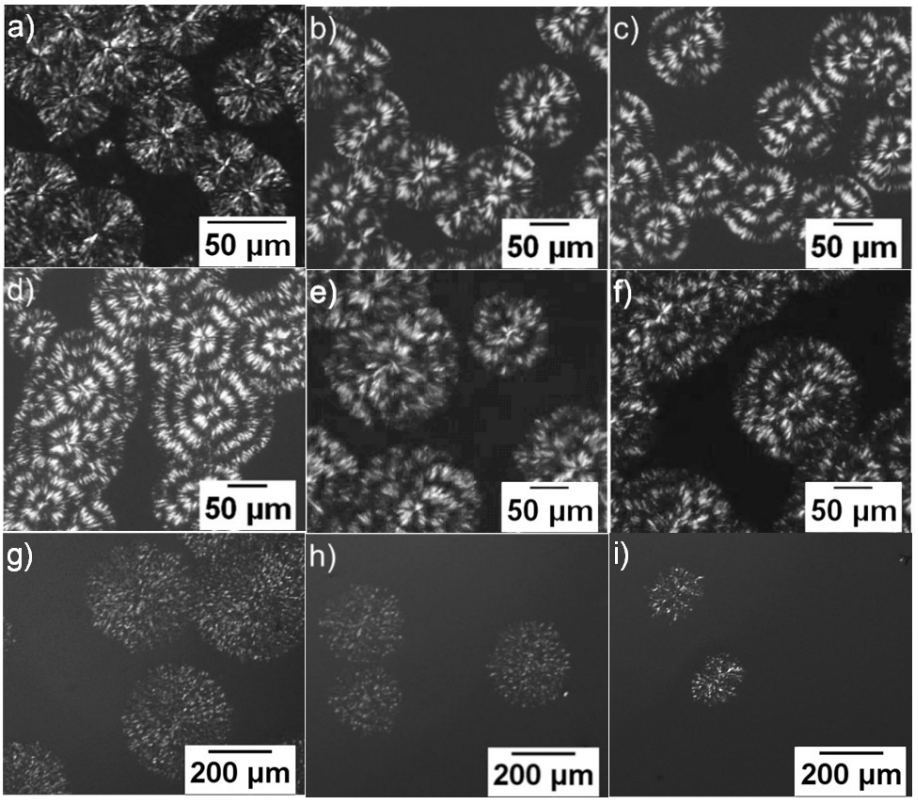

Figure 2. POM images of SPU111 crystallized at different temperatures: (a) 75 °C; (b) 80 °C; (c) 85 °C; (d) 90 °C; (e) 95 °C; (f) 100 °C; (g) 105 °C; (h) 110 °C; (i) 115 °C. The spherulites are constituted of PLLA.

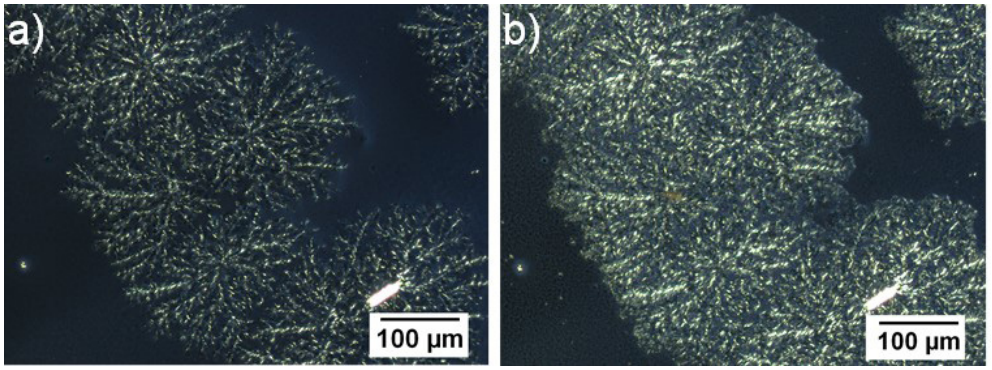

Figure 3. POM images of SPU211, for which PLLA phase was crystallized at (a) 105 °C/1h; (b) and further PEG was crystallized at 40 °C/30 min.

for PEG crystallization. Similar effect observed for the others SPU (Figure S9) and reported for PEG/PLLA blends[31] and PEG-*b*-PLLA[5,9] is attributed to confined PEG crystallization in the PLLA crystalline phase[9-11].

Figure 4 shows POM images (a, b, c, g, h, i) and AFM topography images acquired in tapping mode (d, e, f, j, k, l) for SPU subjected to PLLA isothermal crystallization at 100 °C/1h, followed by PEG isothermal crystallization at 40 °C/30 min. POM images show the strong influence of SPU composition on the morphology of the crystalline phases. In general, the increase in PLLA mass fraction led to the formation of spherulites with Maltese cross, as can be seen in Figure 4b and Figure 4h for SPU121 and SPU163 with PLLA mass fraction of 0.45 and 0.59, respectively. However, spherulites were not well-defined, possibly due to the random distribution of PLLA segments and the heterogeneity of SPU. The morphology of the crystalline phase of the SPU with PLLA mass fraction around 0.25 was quite different for polymers richer in PTMC (SPU112) and PEG (SPU211), Figure 4c and Figure 4g, respectively. SPU112 was birefringent, however, no defined pattern was observed for the crystalline phase, suggesting a disorderly crystal growth in different directions and at different rates. Moreover, the crystal boundaries were diffuse possibly due to the PTMC partial miscibility with PEG and PLLA[22,23]. The increase in the PEG mass fraction led to a decrease in the PLLA crystallites size for SPU111 (Figure 4a) and SPU211 (Figure 4g), compared with SPU121 (Figure 4b). For SPU299 (Figure 4i), the Maltese cross is absent. However, the crystallite boundary is better defined, probably due to the higher PLLA mass fraction compared to that in SPU112 (Figure 4c).

AFM images present a single crystalline structure, which corroborates the PEG confined crystallization in the PLLA crystalline phase. Besides, the uniform distribution of the crystalline phase observed in AFM topography images suggests that the amorphous phase is distributed in the interlamellar region. A radial growth pattern is barely visible in the AFM topographic image for SPU112 (Figure 4f), that indicates random growth of the lamellae in different directions. On the other hand, a radial growth pattern was observed for SPU163 and SPU299 in topographic images (Figure 4k and Figure 4l). The morphology of the SPU211 crystalline phase in the POM image (Figure 4g), resembles that of distorted spherulites, while AFM topographic image (Figure 4j) reveals axialites that suggests growth in a preferential direction[5]. The presence of axialites in the PEG-*b*-PLLA crystalline phase was due to the changes in the phase separation associated to the increase in the crystallization temperature[37]. The increase of PEG content in SPU might lead to a similar effect on the phase separation of the segments in SPU in response to changes in the temperature. Complementary AFM topographic images are shown in Figures S10.

The kinetics of the crystallization of PLLA segments in the SPU was evaluated by POM and the results are summarized in Table S1, Supplementary Material. This study could not be conducted to PEG segments because it occurred in confined environments of the PLLA crystalline phase.

For homopolymers and copolymers, the nucleation step can be described by the Turnbull and Fisher equation[2,38,39] The nucleation rate for random and block copolymers is lower as compared with their parent homopolymers because of the restrictions imposed by the comonomers and blocks[2]. Impurities and heterogeneities may induce nucleation and increase the nucleation rate at higher temperatures due to heterogeneous nucleation[40,41]. Besides, in copolymers, nucleation rate can be affected by the composition and interfacial energy for multiphase systems[2,38]. As discussed earlier, SPU are multiphase polymers whose phases may be mixtures with diffuse interfaces and different capacities for nucleation of the PLLA.

The nucleation rate of PLLA-diol and PLLA in the SPU and, determined as the slope of the number of nuclei per unit of area *vs.* time plots (Figures S11 and S13), is shown in Figure 5 as a function of crystallization temperature. A bell-shaped profile was not observed for PLLA-diol because it crystallizes in a lower temperature range compared with PLLA segments in the SPU. The maximum nucleation rate for PLLA-diol occurs at temperatures below 75 °C and the nucleation rate (dN/dt) was 12.33 mm^{-2} s^{-1} at 75 °C. On the contrary, for SPU, PLLA nuclei formed at higher temperatures and a lower nucleation rate, due to the presence of amorphous phases with different interfacial energy[2,38] and the lower degree of freedom of the PLLA segments in the SPU chains, respectively. For SPU richer in PLLA, the nucleation rate (dN/dt) *vs.* T_c plots presented the characteristic bell-shape (Figure-5a). The maximum nucleation rate

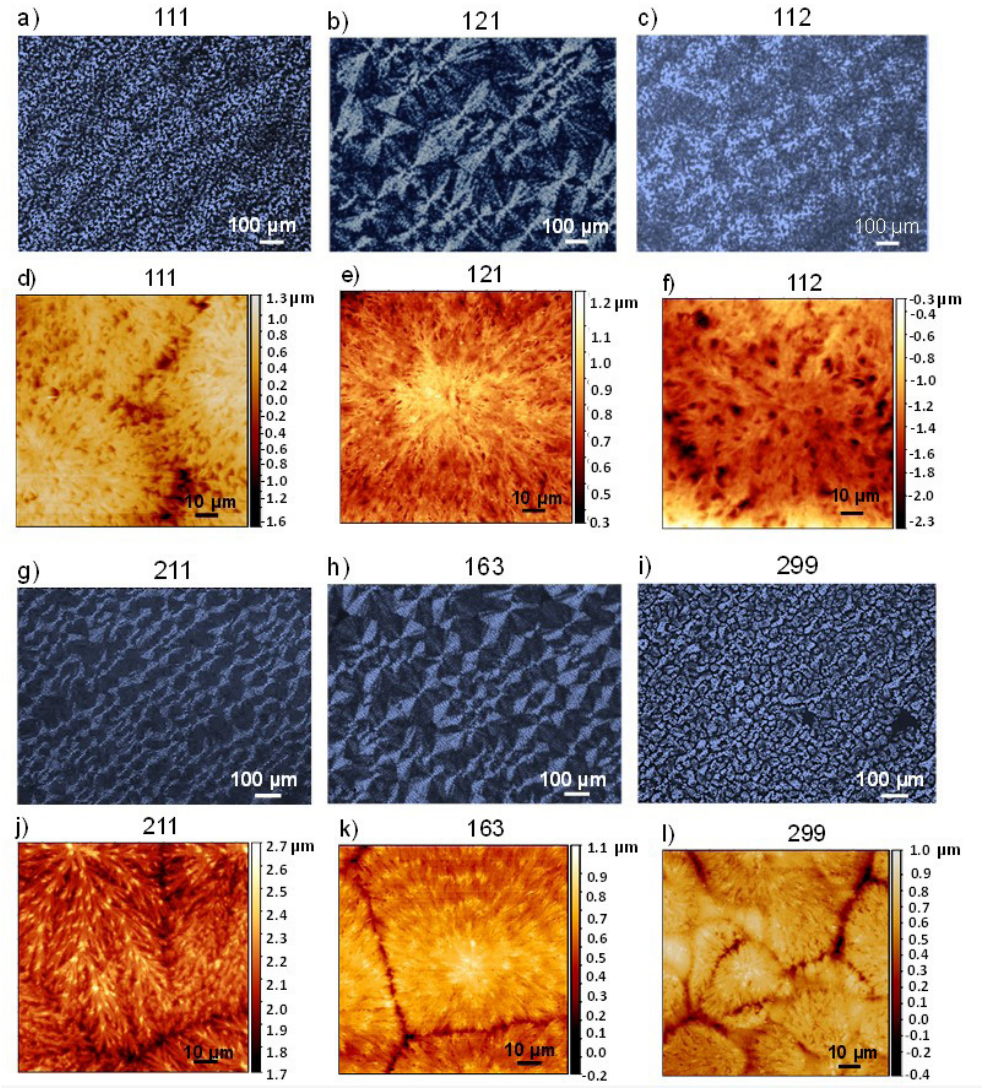

Figure 4. POM and AFM topographic images of the SPU crystallized at 100 °C and further at 40 °C: (a) and (d) SPU111; (b) and (e) SPU121; (c) and (f) SPU112; (g) and (j) SPU211; (h) and (k) SPU163; (i) and (l) SPU299.

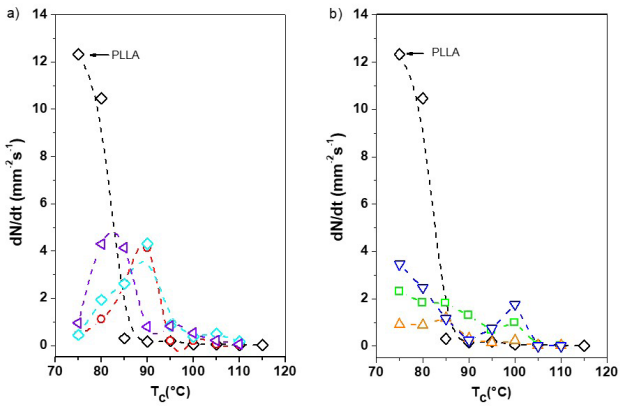

Figure 5. Nucleation rate *vs* T_c for the crystallization of: (a) PLLA (◇), SPU121 (○), SPU163 (◇), and SPU299 (◁); (b) PLLA (◇), SPU112(△), SPU111 (□), and SPU211 (▽). Dotted lines serve to guide the eyes.

occurred at 90 °C for SPU121 and SPU163 and around 80 °C for SPU299. The structural differences such as molar mass and mass fraction of PLLA do not explain the shift of the maximum nucleation rate of the PLLA segments in SPU299 to lower temperatures. However, the SPU global composition is possibly the key to understanding the results. The mass fraction of PEG was 0.25, 0.11 and 0.11 and the mass fraction of PTMC was 0.30, 0.30 and 0.47 for SPU121, SPU163 and SPU299. The concomitant decrease in the PEG mass fraction and the increase in the PTMC mass fraction caused a shift of the maximum nucleation rate in SPU299 to lower temperatures. However, the nucleation rate remained close to ~ 4.0 mm^{-2} s^{-1} – 4.5 mm^{-2} s^{-1} (Figure 5a). These results suggest the mutual cancelation of the antagonistic effects of PEG and PTMC on the nucleation rate of PLLA in the ternary SPU. The nucleation rate for the SPU richer in PLLA was three times lower than the nucleation rate of the PLLA-diol at 75 °C, 12.33 mm^{-2} s^{-1}, an expected result because of the higher diffusion coefficient of PLLA-diol chains.

The nucleation rate *vs.* T_c plots for SPU111, SPU112 and SPU211 presented at least two peaks (Figure 5b), suggesting the occurrence of concurrent nucleation processes in the analyzed temperature range. One hypothesis is that the SPU in the melt is heterogeneous, and nucleation occurs in different phases. However, nucleation occurred uniformly throughout the sample as observed from POM, indicating the absence of the macroscopic phases. Another possibility is that the heterogeneous distribution of PLLA segments in the polyurethane chains and the presence of phases with different compositions and submicrometric dimensions in the amorphous phase could be the causes of the concurrent nucleation processes. Phases of chains with higher PLLA mass fraction could crystallize first, while phases or chains with lower PLLA mass fraction would be segregated from the growth crystal boundary and eventually be crystallized at lower temperatures. In general, the nucleation rate at 100 °C for the SPU with PLLA mass fractions in the range of 0.23 to 0.33 increased with increasing PEG contents in the following order: SPU 112 (x_{PEG} = 0.26; x_{PTMC} = 0.49) < SPU 111 (x_{PEG} = 0.32; x_{PTMC} = 0.35) < SPU 211 (x_{PEG} = 0.44; x_{PTMC} = 0.33). These results differ from those reported in the literature for PEG-*b*-PLLA, in which the dilution effect of the molten PEG phase led to a decrease in the PLLA nucleation rate[12,15]. However, SPU display a more complex phase behavior compared with PEG-*b*-PLLA[29,30]. The partial miscibility and the random distribution of the macrodiols segments in the SPU may influence the kinetics of the crystallization of PLLA.

The growth rate (G) was determined as the slope of the spherulite radius vs time plots (Figures S12 and S14) resulting from monitoring the growth of at least three spherulites. Figure 6 shows the evolution of G in the temperature range of 75-110 °C for the PLLA-diol and SPU. In general, bell-shaped curves were observed with a maximum growth rate in the temperature range of 85-100 °C for SPU, depending on the composition, and at 105 °C for PLLA-diol. For SPU richer in PLLA (Figure 6a), the temperature of maximum growth rate T_{Gmax} increased with the decrease in the PLLA mass fraction: SPU163 (x_{PLLA} = 0.59; T_{Gmax} = 85 °C) > SPU121 (x_{PLLA} = 0.45; T_{Gmax} = 95 °C) > SPU299 (x_{PLLA} = 0.42; T_{Gmax} = 100 °C). For SPU with PLLA mass fraction in the range of 0.23 - 0.33 (SPU211, SPU112 and SPU111), T_{Gmax} was 90 °C and G_{max} was around 0.140-0.148 μm s^{-1} for SPU111 and SPU211 and around 0.090 μm s^{-1} for SPU112 (figure-6b). Curiously, G_{max} values for the SPU richer in PLLA were lower – around 0.120 μm s^{-1}, 0.060 μm s^{-1} and 0.058 μm s^{-1} for SPU121, SPU163 and SPU 299, respectively. Therefore, there was no clear relationship between G_{max} and the PLLA mass fraction in the SPU.

In PEG-*b*-PLLA and PEG/PLLA blends, PEG is miscible with PLLA in the molten state and causes a decrease in the viscosity[10], an increase in the PLLA chains mobility and crystals' growth rate[15,42]. On the other hand, PTMC decreases PLLA mobility in PLLA/PTMC blends and the crystals' growth rate[32]. For SPU, the PLLA, crystallization occurs in presence of both PEG and PTMC segments in a heterogeneous medium in which phases with different compositions coexist. The crescent order of G_{max} observed for SPU richer in PLLA (SPU163 ≅ SPU299 < SPU121) seems correlated to the concomitant increase in the PEG mass fraction and the decrease in the PTMC mass fraction.

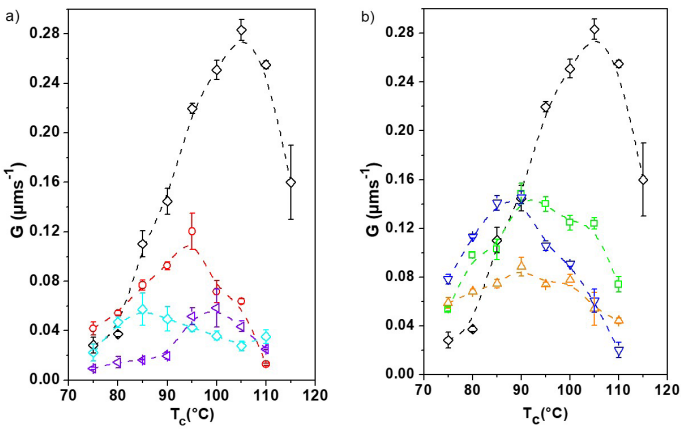

Figure 6. Growth rate *vs* T_c for: (a) PLLA (◇), SPU121 (○), SPU163 (◇), and SPU299 (◁); (b) PLLA (◇), SPU112(△), SPU111 (□), and SPU211 (▽). Dotted lines serve to guide the eyes.

The G_{max} for the crystallization of the PLLA segments in the SPU varied in the range of 0.058μm s^{-1}–0.148μm s^{-1} in the temperature range of 80-100 °C, while that for PLLA homopolymer with comparable molar mass (M_n =1.759 kDa), G_{max} = 0.15μm s^{-1} at T_{Gmax} = 105 °C and for PLLA-diol used in the synthesis of the SPU, G_{max} = 0.283 ± 0.009 μm s^{-1} at 105 °C. This is in agreement with the literature; for random[2,38] and block copolymers[2,12,41,43] the spherulite growth rate is lower compared to the values for analogous homopolymers due to the restrictions of the chain mobility. The PLLA spherulite growth rate for SPU163 and SPU299 of around 0.060 μm s^{-1} at 85 °C and 100 °C, respectively, were close to the ones found for PEG-*b*-PLLA diblock copolymers (0.04 μms^{-1} at 115 °C)[12]. However, the molar mass of the PLLA block in the diblock copolymer was around three times more than the PLLA segment in the SPU. This is possibly due to the random distribution of the PLLA segments in the polymer chains and the multiple amorphous phases of SPU.

4. Conclusions

Despite the random distribution of PLLA, PEG and PTMC segments in SPU chains, PLLA or both PLLA and PEO segments crystallize from the melt. In this condition, PLLA crystallizes first and forms crystalline structures of morphologies such as spherulites with classical Maltese cross, ring banded spherulites, and axialites depending on the composition of the SPU and crystallization temperature. Further cooling leads to a confined PEG crystallization, in which the PLLA crystalline phase acts as a template. The crystallites of the SPU richer in PLLA display a preference for the morphology of spherulites resulting from radial lamellar growth. On the other hand, for SPU richer in PTMC, the growth of the crystallites occurs randomly leading to undefined patterns and diffuse interfaces. The influence of the SPU composition on the kinetics of the crystallization is complex. The isothermal crystallization of PLLA segments is governed by the SPU composition and the distribution of the segments in the chains.

5. Author's Contribution

- **Conceptualization –** Rafael Bergamo Trinca; Maria Isabel Felisberti.
- **Data curation –** André Sanches Bevilacqua; Maria Isabel Felisberti.
- **Formal analysis –** André Sanches Bevilacqua; Rafael Bergamo Trinca; Maria Isabel Felisberti.
- **Funding acquisition –** Maria Isabel Felisberti.
- **Investigation –** André Sanches Bevilacqua; Maria Isabel Felisberti.
- **Methodology –** Rafael Bergamo Trinca; Maria Isabel Felisberti.
- **Project administration –** Maria Isabel Felisberti.
- **Resources –** Maria Isabel Felisberti.
- **Software –** MS Word; Origin 8.1.
- **Supervision –** Maria Isabel Felisberti.
- **Validation –** André Sanches Bevilacqua; Rafael Bergamo Trinca; Maria Isabel Felisberti.
- **Visualization –** Rafael Bergamo Trinca; Maria Isabel Felisberti.
- **Writing – original draft –** André Sanches Bevilacqua.
- **Writing – review & editing –** Rafael Bergamo Trinca; Maria Isabel Felisberti.

6. Acknowledgements

The authors acknowledge FAPESP (Grant number 2015/25406-5) and CAPES (Finance Code 001) for the financial support, and LNNano/CNPEM (proposal AFM-NSIIIa-16677).

7. References

1. Piorkowska, E., & Rutledge, G. C. (Eds.). (2013). *Handbook of polymer crystallization*. Hoboken: John Wiley & Sons, Inc.. http://dx.doi.org/10.1002/9781118541838.
2. Mandelkern, L. (2004). *Crystallization of polymers: kinetics and mechanims*. UK: Cambridge Press. http://dx.doi.org/10.1017/CBO9780511535413.
3. Pu, W.-F., Liu, R., Wang, K.-Y., Li, K.-X., Yan, Z.-P., Li, B., & Zhao, L. (2015). Water-soluble core-shell hyperbranched polymers for enhanced oil recovery. *Industrial & Engineering Chemistry Research*, *54*(3), 798-807. http://dx.doi.org/10.1021/ie5039693.
4. Hsieh, Y.-T., Nurkhamidah, S., & Woo, E. M. (2011). Lamellar orientation and interlamellar cracks in co-crystallized poly(ethylene oxide)/poly(L-lactic acid) blend. *Polymer Journal*, *43*(9), 762-769. http://dx.doi.org/10.1038/pj.2011.63.
5. Huang, S., & Jiang, S. (2014). Structures and morphologies of biocompatible and biodegradable block copolymers. *RSC Advances*, *4*(47), 24566-24583. http://dx.doi.org/10.1039/C4RA03043E.
6. Palacios, J. K., Liu, G., Wang, D., Hadjichristidis, N., & Müller, A. J. (2019). Generating triple crystalline superstructures in melt miscible PEO- b -PCL- b -PLLA triblock terpolymers by controlling thermal history and sequential crystallization. *Macromolecular Chemistry and Physics*, *220*(20), 1900292. http://dx.doi.org/10.1002/macp.201900292.
7. Jing, Z., Huang, X., Liu, X., Liao, M., & Li, Y. (2023). Poly(lactide)-based supramolecular polymers driven by self-complementary quadruple hydrogen bonds: construction, crystallization and mechanical properties. *Polymer International*, *72*(1), 39-53. http://dx.doi.org/10.1002/pi.6445.
8. Castillo, R. V., & Müller, A. J. (2009). Crystallization and morphology of biodegradable or biostable single and double crystalline block copolymers. *Progress in Polymer Science*, *34*(6), 516-560. http://dx.doi.org/10.1016/j.progpolymsci.2009.03.002.
9. Yang, J., Liang, Y., Luo, J., Zhao, C., & Han, C. C. (2012). Multilength scale studies of the confined crystallization in poly(l -lactide)- block -poly(ethylene glycol) copolymer. *Macromolecules*, *45*(10), 4254-4261. http://dx.doi.org/10.1021/ma202505f.
10. Wang, L., Feng, C., Shao, J., Li, G., & Hou, H. (2019). The crystallization behavior of poly(ethylene glycol) and poly(L-lactide) block copolymer: effects of block length of poly(ethylene glycol) and poly(L-lactide). *Polymer Cryslallization*, *2*(4), e10071. http://dx.doi.org/10.1002/pcr2.10071.
11. Hu, D. S.-G., & Liu, H.-J. (1994). Effects of soft segments and hydrolysis on the crystallization behavior of degradable poly(oxyethylene)/poly(L-lactide) block copolymers.

Macromolecular Chemistry and Physics, *195*(4), 1213-1223. http://dx.doi.org/10.1002/macp.1994.021950409.

12. Huang, S., Jiang, S., An, L., & Chen, X. (2008). Crystallization and morphology of poly(ethylene oxide-b-lactide) crystalline-crystalline diblock copolymers. *Journal of Polymer Science. Part B, Polymer Physics*, *46*(13), 1400-1411. http://dx.doi.org/10.1002/polb.21474.
13. Yang, J., Zhao, T., Liu, L., Zhou, Y., Li, G., Zhou, E., & Chen, X. (2006). Isothermal crystallization behavior of the poly(L-lactide) block in poly(L-lactide)-poly(ethylene glycol) diblock copolymers: influence of the PEG block as a diluted solvent. *Polymer Journal*, *38*(12), 1251-1257. http://dx.doi.org/10.1295/polymj.PJ2006094.
14. Huang, S., Li, H., Jiang, S., Chen, X., & An, L. (2011). Morphologies and structures in poly(l-lactide-b-ethylene oxide) copolymers determined by crystallization, microphase separation, and vitrification. *Polymer Bulletin*, *67*(5), 885-902. http://dx.doi.org/10.1007/s00289-011-0518-8.
15. Sun, J., Hong, Z., Yang, L., Tang, Z., Chen, X., & Jing, X. (2004). Study on crystalline morphology of poly(l-lactide)-poly(ethylene glycol) diblock copolymer. *Polymer*, *45*(17), 5969-5977. http://dx.doi.org/10.1016/j.polymer.2004.06.026.
16. Li, F., Hou, J., Zhu, W., Zhang, X., Xu, M., Luo, X., Ma, D., & Kim, B. K. (1996). Crystallinity and morphology of segmented polyurethanes with different soft-segment length. *Journal of Applied Polymer Science*, *62*(4), 631-638. http://dx.doi.org/10.1002/(SICI)1097-4628(19961024)62:4<631::AID-APP6>3.0.CO;2-U.
17. Sonnenschein, M. F., Lysenko, Z., Brune, D. A., Wendt, B. L., & Schrock, A. K. (2005). Enhancing polyurethane properties via soft segment crystallization. *Polymer*, *46*(23), 10158-10166. http://dx.doi.org/10.1016/j.polymer.2005.08.006.
18. Wang, W., Jin, Y., Yang, X., & Su, Z. (2010). Chain orientation and distribution in ring-banded spherulites formed in poly(ester urethane) multiblock copolymer. *Journal of Polymer Science. Part B, Polymer Physics*, *48*(5), 541-547. http://dx.doi.org/10.1002/polb.21919.
19. Hood, M. A., Wang, B., Sands, J. M., La Scala, J. J., Beyer, F. L., & Li, C. Y. (2010). Morphology control of segmented polyurethanes by crystallization of hard and soft segments. *Polymer*, *51*(10), 2191-2198. http://dx.doi.org/10.1016/j.polymer.2010.03.027.
20. Fernández-d'Arlas, B., Baumann, R. P., Pöselt, E., & Müller, A. J. (2017). Influence of composition on the isothermal crystallization of segmented thermoplastic polyurethanes. *CrystEngComm*, *19*(32), 4720-4733. http://dx.doi.org/10.1039/C7CE01028A.
21. Król, P. (2007). Synthesis methods, chemical structures and phase structures of linear polyurethanes. Properties and applications of linear polyurethanes in polyurethane elastomers, copolymers and ionomers. *Progress in Materials Science*, *52*(6), 915-1015. http://dx.doi.org/10.1016/j.pmatsci.2006.11.001.
22. Trinca, R. B., & Felisberti, M. I. (2015). Segmented polyurethanes based on poly(l-lactide), poly(ethylene glycol) and poly(trimethylene carbonate): physico-chemical properties and morphology. *European Polymer Journal*, *62*, 77-86. http://dx.doi.org/10.1016/j.eurpolymj.2014.11.008.
23. Trinca, R. B., & Felisberti, M. I. (2015). Effect of diisocyanates and chain extenders on the physicochemical properties and morphology of multicomponent segmented polyurethanes based on poly(l-lactide), poly(ethylene glycol) and poly(trimethylene carbonate). *Polymer International*, *64*(10), 1326-1335. http://dx.doi.org/10.1002/pi.4920.
24. Fonseca, L. P., Trinca, R. B., & Felisberti, M. I. (2018). Amphiphilic polyurethane hydrogels as smart carriers for acidic hydrophobic drugs. *International Journal of Pharmaceutics*, *546*(1-2), 106-114. http://dx.doi.org/10.1016/j.ijpharm.2018.05.034. PMid:29772283.
25. Paiva, G. M. S., Duarte, L. G. T. A., Faleiros, M. M., Atvars, T. D. Z., & Felisberti, M. I. (2020). Z-E isomerization of azobenzene based amphiphilic poly(urethane-urea)s: influence on the dynamic mechanical properties and the effect of the self-assembly in solution on the isomerization kinetics. *European Polymer Journal*, *127*, 109583. http://dx.doi.org/10.1016/j.eurpolymj.2020.109583.
26. Fonseca, L. P., Zanata, D. M., Gauche, C., & Felisberti, M. I. (2020). A one-pot, solvent-free, and controlled synthetic route for thermoresponsive hyperbranched polyurethanes. *Polymer Chemistry*, *11*(39), 6295-6307. http://dx.doi.org/10.1039/D0PY01026J.
27. Paiva, G. M. S., Duarte, L. G. T. A., Faleiros, M. M., Atvars, T. D. Z., & Felisberti, M. I. (2021). Photoactive polyurethanes based on 2,2′-dihydroxyazobenzene fluorescent segments. *Journal of Molecular Liquids*, *337*, 116481. http://dx.doi.org/10.1016/j.molliq.2021.116481.
28. Bronzeri, L. B., Gauche, C., Gudimard, L., Courtial, E.-J., Marquette, C., & Felisberti, M. I. (2021). Amphiphilic and segmented polyurethanes based on poly(ε-caprolactone)diol and poly(2-ethyl-2-oxazoline)diol: synthesis, properties, and a preliminary performance study of the 3D printing. *European Polymer Journal*, *151*, 110449. http://dx.doi.org/10.1016/j.eurpolymj.2021.110449.
29. Panwiriyarat, W., Tanrattanakul, V., Pilard, J.-F., Pasetto, P., & Khaokong, C. (2013). Effect of the diisocyanate structure and the molecular weight of diols on bio-based polyurethanes. *Journal of Applied Polymer Science*, *130*(1), 453-462. http://dx.doi.org/10.1002/app.39170.
30. Caracciolo, P. C., Buffa, F., & Abraham, G. A. (2009). Effect of the hard segment chemistry and structure on the thermal and mechanical properties of novel biomedical segmented poly(esterurethanes). *Journal of Materials Science. Materials in Medicine*, *20*(1), 145-155. http://dx.doi.org/10.1007/s10856-008-3561-8. PMid:18704646.
31. Rufino, T. C., & Felisberti, M. I. (2016). Confined PEO crystallisation in immiscible PEO/PLLA blends. *RSC Advances*, *6*(37), 30937-30950. http://dx.doi.org/10.1039/C6RA02406H.
32. Zhao, L.-F., Cheng, J., Tian, X.-J., & Zhang, R.-L. (2015). Miscibility and isothermal crystallization of poly(L-lactide) and poly(trimethylene carbonate) blends. *Chinese Journal of Polymer Science*, *33*(3), 499-507. http://dx.doi.org/10.1007/s10118-015-1604-4.
33. Kim, J.-H., & Lee, J. H. (2002). Preparation and properties of poly(L-lactide)-block-poly(trimethylene carbonate) as biodegradable thermoplastic elastomer. *Polymer Journal*, *34*(3), 203-208. http://dx.doi.org/10.1295/polymj.34.203.
34. Barbosa, P. C., Rodrigues, L. C., Silva, M. M., Smith, M. J., Parola, A. J., Pina, F., & Pinheiro, C. (2010). Solid-state electrochromic devices using PTMC/PEO blends as polymer electrolytes. *Electrochimica Acta*, *55*(4), 1495-1502. http://dx.doi.org/10.1016/j.electacta.2009.03.031.
35. Trinca, R. B., & Felisberti, M. I. (2014). Influence of the synthesis conditions on the structural and thermal properties of poly(l -lactide)- b -poly(ethylene glycol)- b -poly(l -lactide). *Journal of Applied Polymer Science*, *131*(13), 40419. http://dx.doi.org/10.1002/app.40419.
36. Trinca, R. B., Abraham, G. A., & Felisberti, M. I. (2015). Electrospun nanofibrous scaffolds of segmented polyurethanes based on PEG, PLLA and PTMC blocks: physico-chemical properties and morphology. *Materials Science and Engineering C*, *56*, 511-517. http://dx.doi.org/10.1016/j.msec.2015.07.018. PMid:26249621.

37. Li, B., Marand, H., & Esker, A. R. (2007). Dendritic growth of poly(ε-caprolactone) crystals from compatible blends with poly(t-butyl acrylate) at the air/water interface. *Journal of Polymer Science. Part B, Polymer Physics*, *45*(24), 3200-3318. http://dx.doi.org/10.1002/polb.21328.

38. Safari, M., Mugica, A., Zubitur, M., Martínez de Ilarduya, A., Muñoz-Guerra, S., & Müller, A. J. (2019). Controlling the isothermal crystallization of isodimorphic PBS-ran-PCL random copolymers by varying composition and supercooling. *Polymers*, *12*(1), 17. http://dx.doi.org/10.3390/polym12010017. PMid:31861773.

39. Umemoto, S., Hayashi, R., Kawano, R., Kikutani, T., & Okui, N. (2003). Molecular weight dependence of primary nucleation rate of poly(ethylene succinate). *Journal of Macromolecular Science - Physics. Journal of Macromolecular Science, Part B: Physics*, *42*(3-4), 421-430. http://dx.doi.org/10.1081/MB-120021571.

40. Khariwala, D. U., Taha, A., Chum, S. P., Hiltner, A., & Baer, E. (2008). Crystallization kinetics of some new olefinic block copolymers. *Polymer*, *49*(5), 1365-1375. http://dx.doi.org/10.1016/j.polymer.2007.12.046.

41. Andjelić, S., Jamiolkowski, D., McDivitt, J., Fischer, J., & Zhou, J. (2001). Spherulitic growth rates and morphology of absorbable poly(p-dioxanone) homopolymer and its copolymer by hot-stage optical microscopy. *Journal of Polymer Science. Part B, Polymer Physics*, *39*(24), 3073-3089. http://dx.doi.org/10.1002/polb.10065.

42. Yang, J.-M., Chen, H.-L., You, J.-W., & Hwang, J. C. (1997). Miscibility and crystallization of poly(L-lactide)/poly(ethylene glycol) and poly(L-lactide)/poly(ε-caprolactone) blends. *Polymer Journal*, *29*(8), 657-662. http://dx.doi.org/10.1295/polymj.29.657.

43. Wu, H., & Qiu, Z. (2012). Synthesis, crystallization kinetics and morphology of novel poly(ethylene succinate-co-ethylene adipate) copolymers. *CrystEngComm*, *14*(10), 3586-3595. http://dx.doi.org/10.1039/c2ce06629g.

Received: Jan. 04, 2023
Revised: Feb. 27, 2023
Accepted: Mar. 10, 2023

Supplementary Material

Supplementary material accompanies this paper.

Figure S1. a) Storage modulus (E'); b) loss modulus (E") and c) loss factor (tan delta) as a function of temperature for: SPU111 (□); SPU121(○); SPU112(△); SPU211 (▽); SPU163 (◇), and SPU299 (◁).

Figure S2. AFM phase-contrast images for SPU crystallized at 100°C and further at 40°C: a) SPU 111, b) SPU121, c) SPU112, d) SPU211, e) SPU163 and f) SPU299.

Figure S3. POM imagens of the SPU211 crystallized at different temperatures: (a) 75°C, (b) 80°C, (c) 85 °C, (d) 90°C, (e) 95°C, (f) 100°C, (g) 105°C, (h) 110°C and (i) 115°C. The spherulites are constituted of PLLA.

Figure S4. POM imagens of the SPU121 crystallized at different temperatures: (a) 75°C, (b) 80°C, (c) 85 °C, (d) 90°C, (e) 95°C, (f) 100°C, (g) 105°C, (h) 110°C and (i) 115°C. The spherulites are constituted of PLLA.

Figure S5. POM imagens of the SPU112 crystallized at different temperatures: (a) 75°C, (b) 80°C, (c) 85 °C, (d) 90°C, (e) 95°C, (f) 100°C, (g) 105°C, (h) 110°C and (i) 115°C. The spherulites are constituted of PLLA.

Figure S6. POM images of the PLLA-diol crystallized at different temperatures and time, as indicated in each image.

Figure S7. POM imagens of the SPU163 crystallized at different temperatures: (a) 75°C, (b) 80°C, (c) 85 °C, (d) 90°C, (e) 95°C, (f) 100°C, (g) 105°C, (h) 110°C and (i) 115°C. The spherulites are constituted of PLLA.

Figure S8. POM imagens of the SPU299 crystallized at different temperatures: (a) 75°C, (b) 80°C, (c) 85 °C, (d) 90°C, (e) 95°C, (f) 100°C, (g) 105°C, (h) 110°C and (i) 115°C. The spherulites are constituted of PLLA.

Figure S9. POM images after the PLLA crystallization at 100°C/1h for a) SPU 111, c) SPU121, e) SPU112, g) SPU211, i) SPU163 and k) SPU299 and their respective surfaces after PEG crystallization at 40°C in b), d), f), h), j) and l).

Figure S10. AFM topographic images of the SPU crystalized at TcPLLA = 100 °C and TcPEG = 40 °C: a) SPU111, b) SPU121, c) SPU112, d) SPU211, e) SPU163 and f) SPU299.

Figure S11. Number of the PLLA-diol nuclei per area vs. time (N/A vs. t). The crystallization temperature is indicated for each isotherm.

Figure S12. PLLA spherulite radius vs. time curves of the PLLA-diol. The crystallization temperature is indicated for each isotherm.

Figure S13. Number of the PLLA nuclei per area vs. time (N/A vs. t) plots for SPU a) 111, b)121, c) 112, d) 211, e) 163 and f) 299 crystallized at temperatures in the range of 75 - 110°C. The temperature of the crystallization is indicated for each isotherm.

Figure S14. PLLA spherulite radius vs. time plots for a) SPU111, b) SPU121, c) SPU112, d) SPU211, e) SPU163 and f) SPU299 during crystallization in the temperature range of 75 - 110°C. The temperature of the crystallization is indicated for each isotherm.

Table S1. Nucleation and crystal growth rates of the crystallization of the PLLA segments in the SPU.

This material is available as part of the online article from https://doi.org/10.1590/0104-1428.20220123